Planar and axial coherent bremsstrahlung of type *A* from a 17-MeV electron beam in a diamond crystal

K. Chouffani*
Beam Physics and Engineering RIKEN, 2-1 Hirosawa, Wako-Shi, Saitama 351-6198, Japan

I. Endo
Graduate School of Advanced Sciences of Matter, Hiroshima University, Kagamiyama 1-3-1, Higashi-Hiroshima 739-8526, Japan

H. Überall
Physics Department, The Catholic University of America, Washington, DC 20064

(Received 11 July 2000; published 14 June 2001)

Making use of the many-beam (one- and two-dimensional quantum treatment) formalism for transversely bound electrons moving through crystal lattices, we have computed planar and axial coherent bremsstrahlung (type *A*) spectra for 17-MeV electrons passing through a 10-μm thick diamond (*C*) crystal. We found that in the planar case the momentum transfer occurs in the direction perpendicular to the plane and results in a photon emission in the forward direction (electron-beam direction). In the axial case, the momentum transfer occurs in the plane perpendicular to the axis of interest. Only momentum transfers along the scan direction (electron transverse momentum direction) result in a photon emission in the forward direction. Two different scans have shown that the energies of the coherent bremsstrahlung peaks depend strongly on the direction of the electron transverse momentum but the intensities of the strongest peaks do not show any considerable change.

DOI: 10.1103/PhysRevB.64.014304 PACS number(s): 41.60.−m, 78.70.En, 78.90.+t

I. INTRODUCTION

Coherent bremsstrahlung (CB) is somewhat related to channeling radiation (CR) Ref. 1 since both radiations result from the correlated deflections of the incoming particle by atoms in crystalline rows or planes. However, they remain two different processes. Apart from the fact that CR results from the periodic motion of the incident particle inside the crystal lattice while CB is induced by the periodic crossing of the atomic planes, one of the differences is the angle of incidence, i.e., the angle between the incoming particle and a crystal plane or axis. At small angles, comparable to the critical angle θ_c, it was shown[2,3] that CB and CR are simultaneously observed. As the angle is increased beyond θ_c, CR transitions vanish and the x-ray spectrum is entirely dominated by CB.[4] In a quantum-mechanical treatment, CR and CB result from the transition between bound-bound and free-free states belonging to the continuum, respectively. Andersen *et al.*[2] have shown that a quantum treatment of CB (momentum transfer to the lattice) agrees very well with the Born approximation method.

II. THEORETICAL CALCULATIONS

A quantum treatment of CR and CB is based on solving the Dirac equation, which, neglecting the spin interaction when compared to the dipole matrix, reduces to the Schrödinger wave equation

$$\left[\frac{-\hbar^2}{2\gamma m_e}\nabla_\perp^2 + V(\mathbf{r}_\perp)\right]\psi(\mathbf{r}_\perp) = E_\perp \psi(\mathbf{r}_\perp), \tag{1}$$

where $\hbar$ is the Planck constant, m_e the electron mass, γ the ratio of the electron energy and the electron rest mass, $E_\perp$ the electron transverse energy, and $\mathbf{r}_\perp$ the electron position along the transverse direction (one-dimensional for the planar case and two-dimensional for the axial case, respectively). $\psi(\mathbf{r}_\perp)$ is the electron wave function and $\nabla_\perp^2$ the transverse Laplacian. V is the transverse crystal continuum potential obtained by averaging the potential over the crystalline longitudinal direction. The theoretical values of energy lines and linewidths are derived from the ''many-beam'' formalism introduced by Andersen *et al.*[2] The continuum potential is expanded as a Fourier series and the wave functions become Bloch functions and are given by

$$V(\mathbf{r}_\perp) = \sum_{\mathbf{g}_m} V_{\mathbf{g}_m} \exp(i\mathbf{g}_m \cdot \mathbf{r}_\perp),$$

$$\psi_n(\mathbf{r}_\perp) = \frac{1}{\sqrt{A}} \exp(i\mathbf{k}_\perp \cdot \mathbf{r}_\perp) \sum_{\mathbf{g}_m} C_{\mathbf{g}_m}^n \exp(i\mathbf{g}_m \cdot \mathbf{r}_\perp). \tag{2}$$

$\mathbf{g}_m$ and $\mathbf{k}_\perp$ are the reciprocal-lattice vectors and the electron wave vector normal to the crystalline direction, A is a normalizing constant, and the coefficients $C_{\mathbf{g}_m}^n$ are determined from Eq. (1). $V_{\mathbf{g}m}$ are the continuum potential coefficients and are given by[5]

$$V_{\mathbf{g}_m} = -2\pi a_0 e^2 \rho_0 \cos(\mathbf{g}_m \cdot \mathbf{d}) \times \sum_j a_j \exp[-0.25(b_j/4\pi^2 + \rho_{\text{th}}^2)|\mathbf{g}_m|^2]. \tag{3}$$

a_j and b_j are the coefficients used in the fit to the electron-scattering form factor, a_0 is the Bohr radius, e the electron

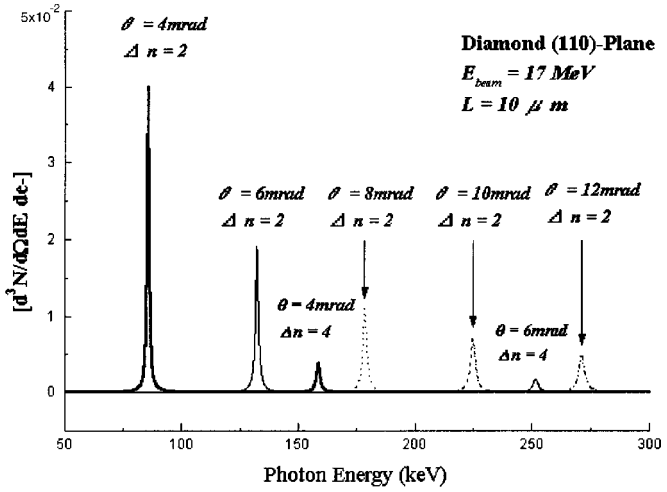

FIG. 1. Planar CB spectra in diamond crystal containing first- and second-order CB for $\theta = 4$, 6, 8, 10, and 12 mrad.

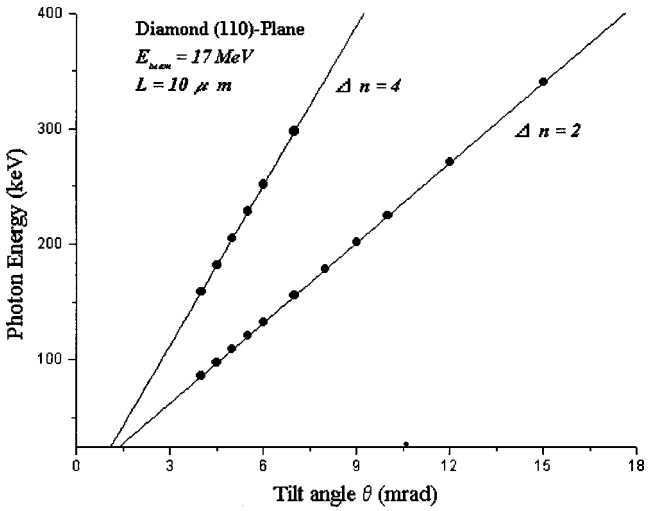

FIG. 2. CB energy dependence on the tilt angle for the respective momentum transfer $g = 4\sqrt{2}\pi/a_p$ for the first order, and $g = 8\sqrt{2}\pi/a_p$ for the second order, together with Eq. (7).

charge, ρ_0 the atomic density, and $\rho_{\rm th}$ the thermal displacement. **d** takes into account the planar (axial) spacing for the (111) plane ($\langle 110\rangle$ axis).

The transition rate per unit thickness, per electron, solid angle, and unit photon energy for a spontaneous transition between the initial state ψ_i and final state ψ_f in the laboratory frame is derived from the Fermi golden rule and is given by

$$\frac{d^4\sigma_{i-f}}{dE_\gamma d e d L d\Omega_\gamma} = \frac{\alpha \lambda\!\!\!^{-2}}{\pi\hbar c}\,\frac{E_\gamma}{2\gamma^2(1-\beta\cos\theta_e)}\,|\langle\psi_f|\nabla_\perp|\psi_i\rangle|^2 \times\left[\sin^2\phi+\left(\frac{\cos\theta_e-\beta}{1-\beta\cos\theta_e}\right)^2\cos^2\phi\right] \times\delta\left(E_\gamma-\frac{\varepsilon_f-\varepsilon_i}{1-\beta\cos\theta_e}\right)P_i(L), \tag{4}$$

where α is the fine-structure constant, c is the speed of light, β is the electron velocity, $\lambda\!\!\!^{-}$ is the Compton wavelength, L is the crystal thickness, θ_e is the angle between the photon wave vector and the electron direction, and ϕ is the azimuthal angle. E_γ is the photon energy and ε_i and ε_f are the initial and final energy-level solutions respectively, of Eq. (1). $P_i(L)$ is the population of the initial state as a function of the crystal thickness; in our calculation we have assumed that the population is equal to the initial population, i.e., the population at the surface of the crystal is equal to $|C^i_{\mathbf{g}_m=\mathbf{0}}|^2$. The dipole matrix element $\langle\psi_f|\nabla_\perp|\psi_i\rangle$, which describes the strength of the spontaneous transition, is given by

$$\langle\psi_f|\nabla_\perp|\psi_i\rangle=\sum_{\mathbf{g}_m} C^f_{\mathbf{g}_m}C^i_{\mathbf{g}_m}(\mathbf{g}_m+\mathbf{k}_\perp). \tag{5}$$

Several line-broadening mechanisms modify the δ function to an approximate Lorentzian shape.[6] In our calculations the full width at half maximum of the CB peaks was obtained as the quadrature summation of the widths due to the finite crystal thickness and incoherent scattering of electrons on phonons[7] only. The incoherent scattering contribution to the linewidth for free-to-free transition was determined by fitting the widths for bound-to-bound states and extending them to higher-energy lines. We have not included the effect of the electron-beam divergence ($\theta_{\rm div}$) and multiple scattering ($\theta_{\rm ms}$) but it can readily be done by convoluting the Lorentzian distributions with a Gaussian angular distribution[8] of width equal to $\sqrt{\theta^2_{\rm div}+\theta^2_{\rm ms}}$. We will only show CB spectra on the (110) plane and the $\langle 100\rangle$, $\langle 110\rangle$ axes for the diamond crystal but the formulas can be used for any orientation and diamond-structure-like targets.

III. RESULTS AND DISCUSSION

For 17-MeV electrons in a 10-μm diamond target, the critical angle is between 1 and 4 mrad. In order to reach a linear dependence between CB energy lines and the tilt angle such that neither bound-to-bound nor free-to-bound transitions are possible, the tilt angle was taken greater than 4 and 6 mrad for planar and axial calculations, respectively. Going to higher angles enables us to reduce the number of decaying states, and therefore allows a limited number of states to reach maximum population (one and two states for planar and axial cases, respectively). The number of beams, i.e., number of reciprocal-lattice vectors, depends on the choice of orientation (axial or planar) and the choice of target (depth of continuum potential). For the planar case, in order to achieve proper eigenvalue, dipole matrices, and eigenvector components convergence, 101 beams are required (up to 12 mrad), while for the $\langle 100\rangle$ and $\langle 110\rangle$ axes more than 3281 beams are required for the same angle. It is helpful to know that the energy levels of the quantum states and dipole matrices [Eq. (5)] of the transitions are periodic with period $\mathbf{g}_p$ the smallest magnitudewise reciprocal vector parallel to the scan or transverse electron momentum direction. This enabled us to run the many-beam code at very small angles but it is still necessary to run the code at the angle of interest in order to find the energy and the population of the initial state. Even though we have used the Born approximation (modi-

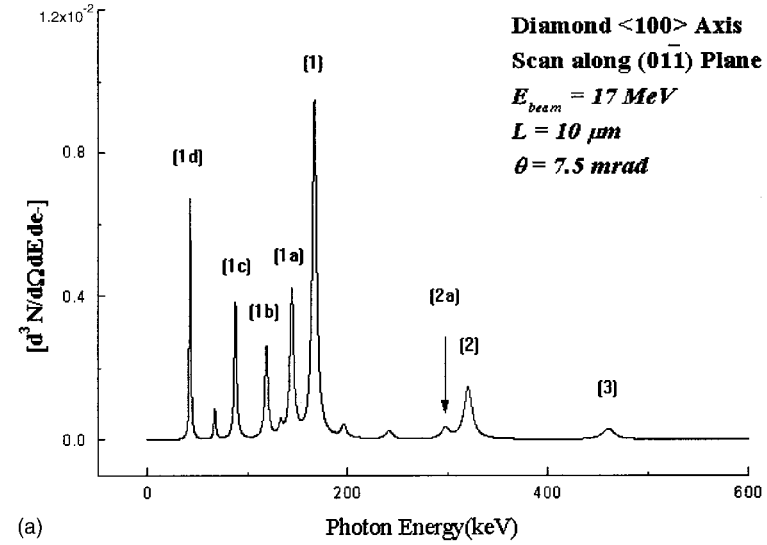

(a)

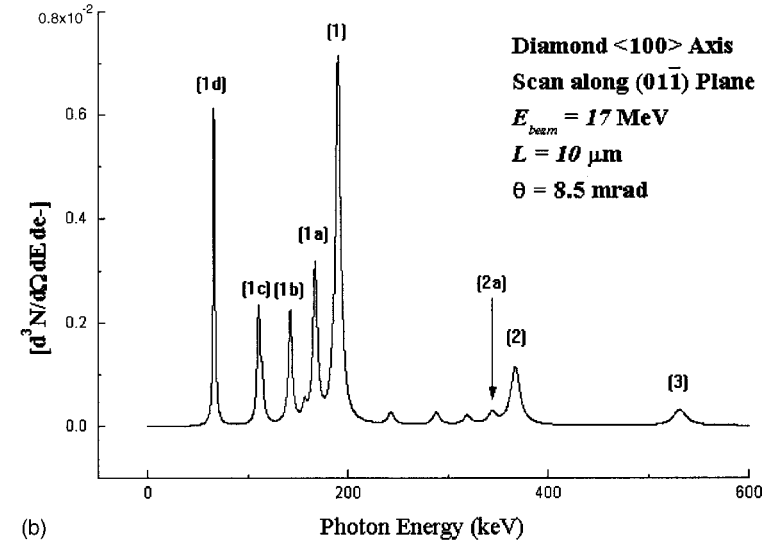

(b)

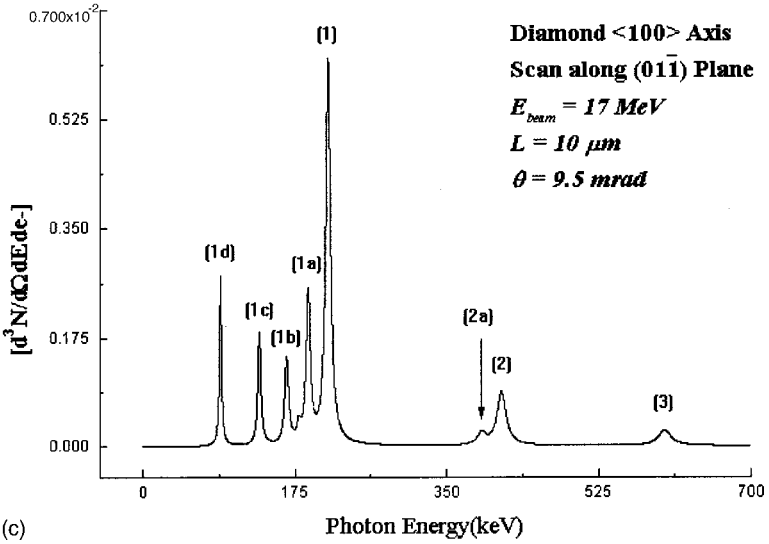

(c)

FIG. 3. (a) (b) and (c) CB axial spectra for the ⟨100⟩ axis at $\theta = 7.5$, 8.5, and 9.5 mrad for a scan taken along the $(01\bar{1})$ plane. For every CB order, all CB peaks are located below the CB peak for which the allowed momentum transfer has the smallest magnitude as can be seen from Eq. (7). Therefore, second-order CB peaks can be found mixed with first-order CB peaks (see text for explanations).

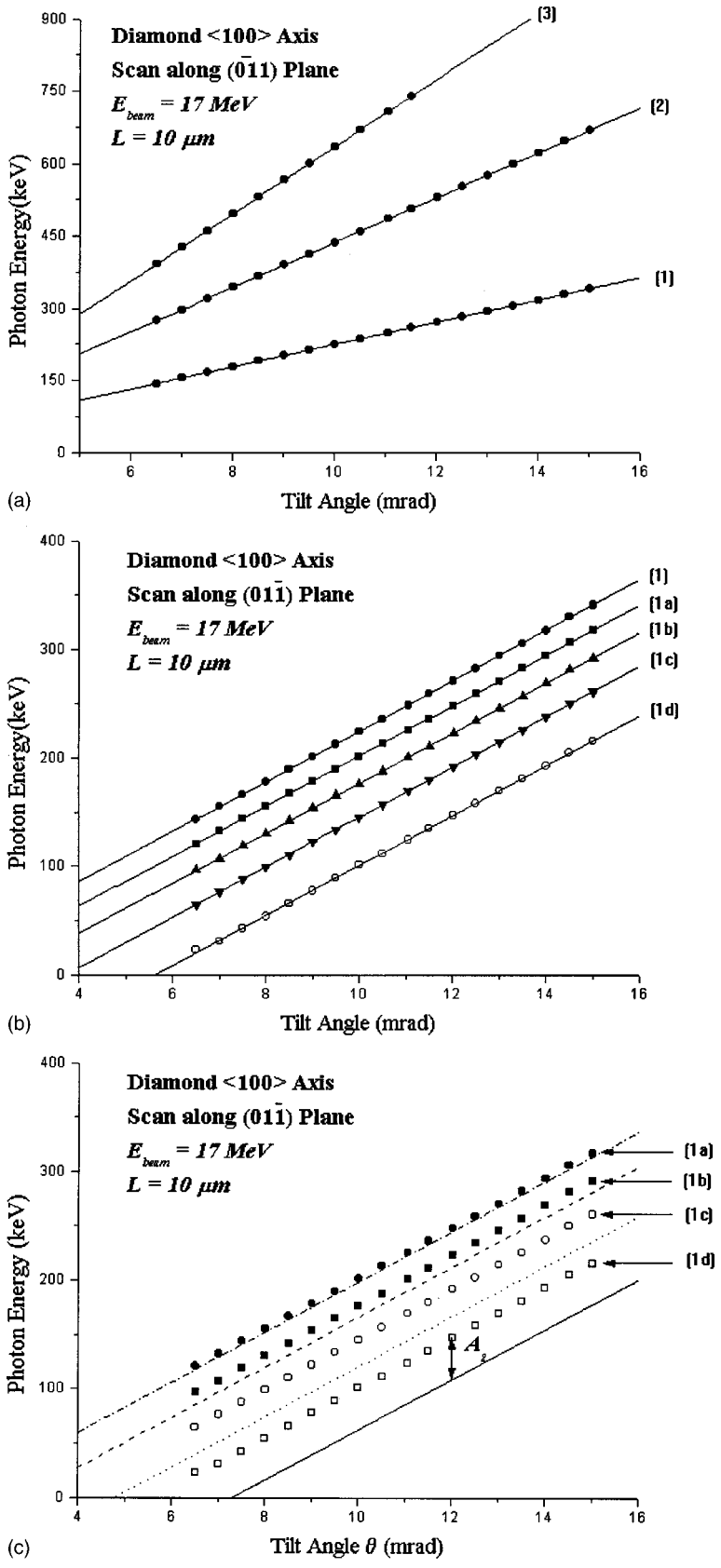

FIG. 4. (a) Photon energy versus the tilt angle for the peaks labeled (1), (2), and (3). The solid lines represent Eq. (7) for $\mathbf{g}_{n,n}=2n(\mathbf{g}_{0,1,0}+\mathbf{g}_{0,0,1})$, with n equal to 1, 2, and 3 for first (1), second (2), and third (3) CB order, respectively. (b) Photon energies of first-order CB peaks versus the tilt angle. The solid lines are fits to the data points. (c) Photon energies of first-order CB peaks versus the tilt angle. The dash-dotted, dashed, dotted, and solid lines represent Eq. (7) with momentum transfer $(6,-2)$, $(8,-4)$, $(10,-6)$, and $(12,-8)$, respectively.

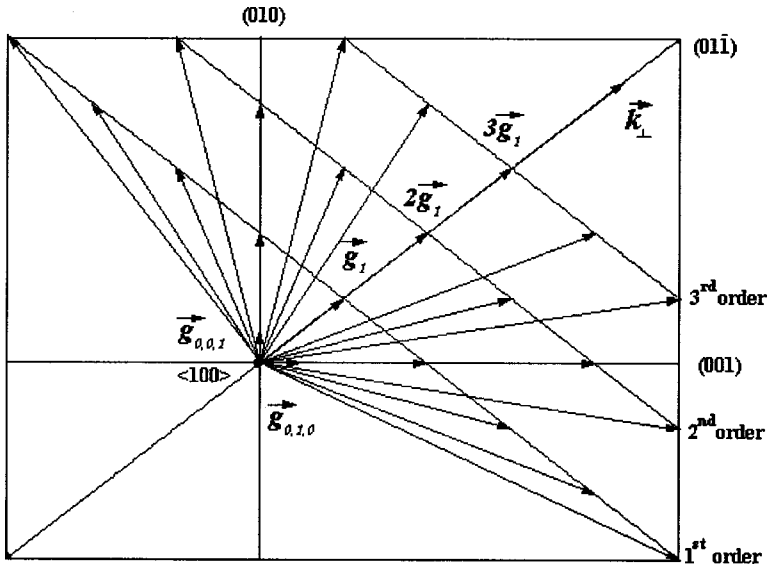

FIG. 5. CB momentum-transfer vector directions for the first three CB orders.

fied formulas of Ref. 2 for the axial case) to identify the momentum-transfer vectors, we will only present the calculations from the many-beam formalism. In the axial calculations the electron-beam direction is parallel to the plane containing the axis of interest. We have used the conventional picture of CB by considering the emission of a photon and a simultaneous momentum transfer $\mathbf{g}_n$ in the transverse plane and axis in the case of axial and planar CB, respectively. Using the energy- and momentum-conservation equation, the photon energy E_γ is given by

$$E_\gamma = \frac{(\hbar c)^2[\mathbf{k}\cdot\mathbf{g}_n - g_n^2/2]}{E+\hbar c\mathbf{u}_\gamma^{\parallel}\cdot(\mathbf{g}_n-\mathbf{k})} + E_\gamma^{\perp}\frac{\hbar c\mathbf{u}_\gamma^{\perp}\cdot(\mathbf{k}-\mathbf{g}_n)}{E+\hbar c\mathbf{u}_\gamma^{\parallel}\cdot(\mathbf{g}_n-\mathbf{k})}$$
$$\approx \frac{2\gamma(\hbar c)^2}{m_e c^2}[\mathbf{k}\cdot\mathbf{g}_n - g_n^2/2] + \frac{2\gamma\hbar c}{m_e c^2}E_\gamma^{\perp}\mathbf{u}_\gamma^{\perp}\cdot(\mathbf{k}-\mathbf{g}_n). \tag{6}$$

In the equation above, we have assumed that the photon transverse energy $E_\gamma^{\perp}$ is small compared to its longitudinal one. $\mathbf{k}$ is the electron momentum; $\mathbf{k}\cdot\mathbf{g}_n = \mathbf{k}_\perp\cdot\mathbf{g}_n$, where $k_\perp \approx k\theta$ is the electron transverse momentum and θ the tilt angle; $\mathbf{u}_\gamma^{\parallel}$ and $\mathbf{u}_\gamma^{\perp}$ are the photon longitudinal and transverse directions, respectively; and E is the electron total energy. For photons emitted in the forward direction, the energy of the photon is

$$E_\gamma = \frac{\gamma(\hbar c)^2}{m_e c^2}[2\mathbf{k}_\perp\cdot\mathbf{g}_n - g_n^2]. \tag{7}$$

Figures 1 and 2 show the CB spectra for the (110) plane of the diamond crystal for five different angles and the energy dependence with the tilt angle, respectively. The transverse direction is defined by $\mathbf{u}=(\mathbf{x}+\mathbf{y})/2$. For each angle, the CB fundamental (first order) and overtones correspond to a momentum transfer $mg\mathbf{u}$, respectively. $g=4\sqrt{2}\pi/a_p$ is the smallest reciprocal-lattice vector (magnitudewise) for which the structure factor is not equal to zero, m is a positive integer equal to 1 for the first order, 2 for the second,$\cdots$, and a_p is the lattice constant. All CB transitions result from a single initial state, which has the strongest population. The final state, the state for which the dipole matrix element [Eq. (5)] is large, is such that the difference of state numbers $\Delta n = 2m$. In terms of momentum transfer, this means that the difference of the values of the initial and final electron transverse momentum must be equal to an integer times g in an extended Brillouin zone.[2]

The axial case is somewhat similar to the planar one, since the momentum transfer occurs in the transverse direction, however the photon emission is not always confined to the forward direction. The axis direction was taken along the $\mathbf{x}$ direction, and the transverse direction is spanned by $\mathbf{g}_{0,1,0} = 2\pi/a_p\mathbf{y}$ and $\mathbf{g}_{0,0,1} = 2\pi/a_p\mathbf{z}$. For a clear understanding, the reader is invited to look at Figs. 3, 4, and 5 simultaneously. Figures 3(a), (b) and (c) show CB spectra for $\theta = 7.5$, 8.5, and 9.5 mrad, respectively, for an incident electron transverse momentum along the $(01\bar{1})$ plane, i.e., parallel to $\mathbf{g}_{0,1,0}+\mathbf{g}_{0,0,1}$. The peaks labeled (1), (1a), (1b), (1c), and (1d) correspond to first-order CB transitions with momentum transfers (see explanation below) $\mathbf{g}_{2,2} = 2\mathbf{g}_{0,1,0}+2\mathbf{g}_{0,0,1}$, $\mathbf{g}_{6,-2}$, $\mathbf{g}_{8,-4}$, $\mathbf{g}_{10,-6}$, and $\mathbf{g}_{12,-8}$, respectively. The remaining peaks located below peaks (2) ($\mathbf{g}_{4,4}$) and (2a) ($\mathbf{g}_{8,0}$) are all second-order CB transitions [(2) and (2a) included]. Only a single third-order CB peak is visible and is labeled (3) corresponding to a momentum transfer $\mathbf{g}_{6,6}$. Figure 4(a) shows the energy dependence on the tilt angle for the three peaks labeled (1), (2), and (3) in Fig. 3. The solid lines correspond to Eq. (7) for a momentum transfer $\mathbf{g}_n = 2n(\mathbf{g}_{0,1,0}+\mathbf{g}_{0,0,1})$, where n is a positive integer equal to 1, 2, and 3 for first, second, and third order, respectively. Figure 4(b) shows the energy dependence on the tilt angle for the five major peaks shown in Fig. 3. All straight lines have the same slope as (1); this means that the term $\mathbf{k}_\perp\cdot\mathbf{g}_n/k_\perp$ in Eq. (7), is a constant, i.e., all allowed momentum-transfer vectors are reciprocal-

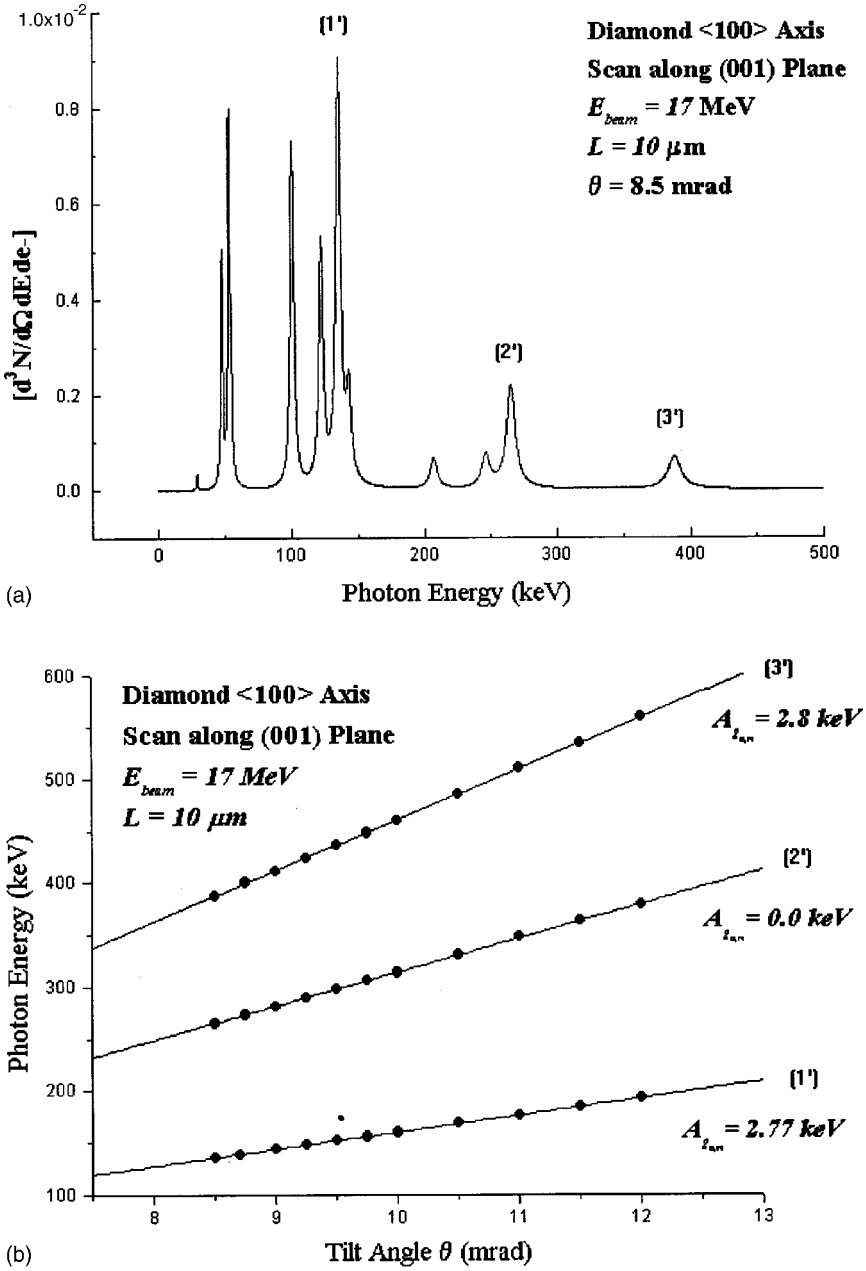

FIG. 6. (a) CB axial spectra for the ⟨100⟩ axis at $\theta = 8.5$ mrad for a scan taken along the (001) plane. In this scan direction no first-order CB results in a photon emission in the forward direction (b) Photon energy of peaks labeled $(1')$, $(2')$, and $(3')$ as a function of the tilt angle and determination of the constants $A_{\mathbf{g}n,m}$ for each transition.

lattice vectors whose tips lie on a straight line perpendicular to the electron transverse momentum as shown in Fig. 5(a). In this example, a first-order transition results in the transfer of a vector $\mathbf{g}_{n,m} = n\mathbf{g}_{0,1,0} + m\mathbf{g}_{0,0,1}$ such that $n+m=4$ and $S_{\mathbf{g}n,m} \neq 0$, where $S_{\mathbf{g}n,m}$ is the structure factor. For second and third order, the condition is $n+m=8$ and 12, respectively. It is worth mentioning that when the electron transverse momentum lies on the edge of a Brillouin zone ($k_\perp / g_p = 0, \pm 0.5, \pm 1, \cdots$, where $\mathbf{g}_p = \mathbf{g}_{2,2}$), all peaks, for which the momentum transfer is not along the direction of the transverse electron momentum, correspond to CB transitions for which the energy level of the final state is doubly degenerate ($\pm l$, where l is the orbital quantum number), and each peak is composed of two lines of equal energies and dipole matrices corresponding to the two allowed transfer vectors as shown in Fig. 5(a). However, in Figs. 3(a), (b), and (c) the electron transverse momentum lies away from the Brillouin-zone edges, a splitting of the final levels occurs, and each CB peak is composed of two very close-lying energy lines but only one transition is dominant, in agreement with the Born approximation method. In Fig. 4(c) Eq. (7) though parallel does not match exactly the data points from the many-beam calculation for the corresponding momentum transfer; it is shifted toward the lower-energy region. Therefore CB transitions for which $m=n>0$ result in a photon emission in the forward direction. The energy lines of these transitions, which result in the transfer of the smallest reciprocal-lattice vector allowed, act like cutoff energies for the rest of the CB transitions of the same order. Equation (6) and Fig. 4 enable us to determine the photon emission angles. From Fig. 4(c) it is clear that the second term in Eq. (6) is a constant $A_{\mathbf{g}n,m}$ that can be determined from the data points. The transverse energy is therefore for the two momentum-transfer vectors

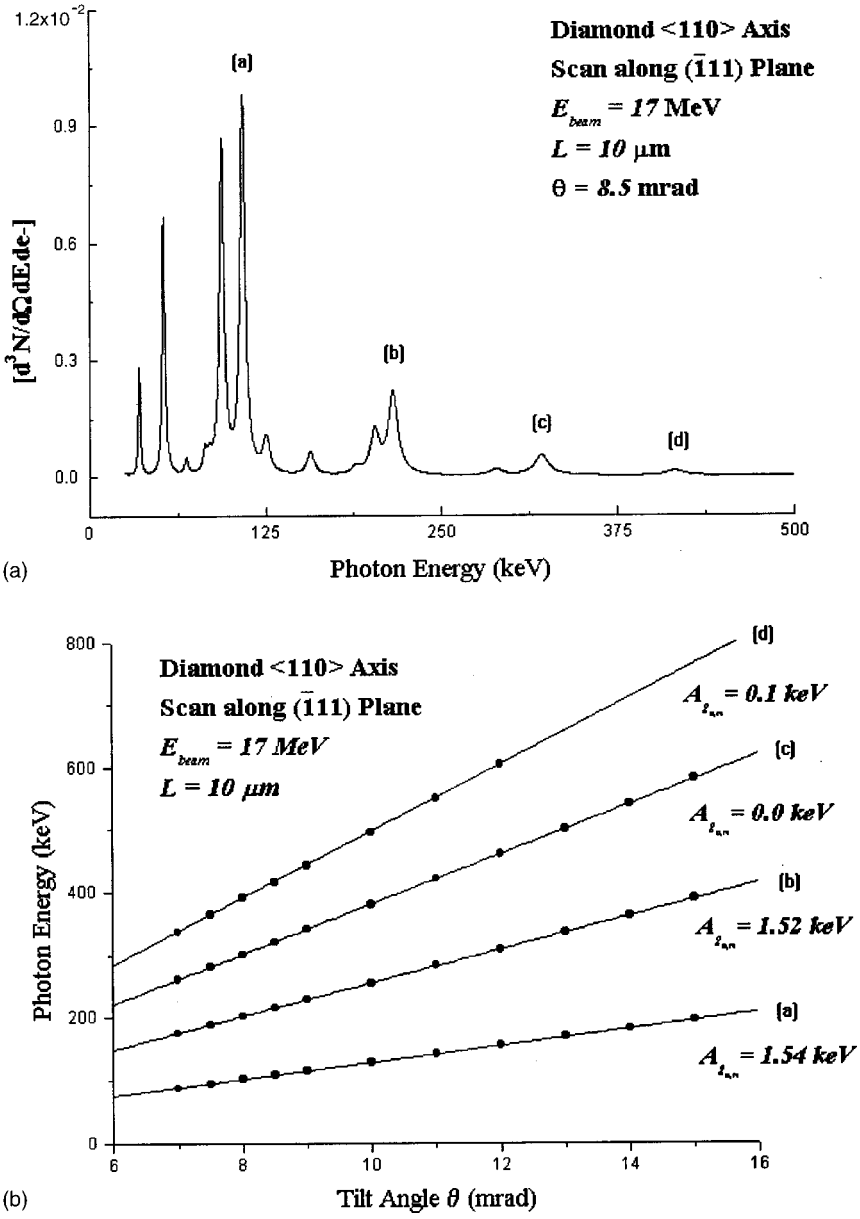

FIG. 7. (a) CB axial spectra for $\langle 110\rangle$ axis at $\theta=8.5$ mrad for a scan taken along the $(\bar{1}11)$ plane. In this scan direction only the third-order CB corresponds to a photon emission in the forward direction. (b) Photon energy as a function of the tilt angle with the corresponding constant [from Eq. (6)].

$$E_\gamma^\perp=\frac{m_e c^2}{2\gamma\hbar c}\,\frac{A_{\mathbf{g}_{n,m}}}{[\mathbf{k}\cos(\mathbf{u}_\gamma^\perp,\mathbf{k}_\perp)\,\theta-g_{n,m}\cos(\mathbf{u}_\gamma^\perp,\mathbf{g}_{n,m})]}\geqslant 0. \tag{8}$$

For $\cos(\mathbf{u}_\gamma^\perp,\mathbf{k}_\perp)>0$, the transverse energy and therefore the emission angle decrease with increasing tilt angle. For $\cos(\mathbf{u}_\gamma^\perp,\mathbf{k}_\perp)=0$, the transverse energy is independent of θ and for each set of allowed momentum-transfer vectors satisfying the two conditions $n+m=4,8,12...$ and $n\neq m$, there exists two transverse opposite photon directions. As an example, we took the first-order (1a) and second-order (2a) peaks corresponding to the momentum-transfer vectors $\mathbf{g}_{6,-2}=6\mathbf{g}_{0,1,0}-2\mathbf{g}_{0,0,1}$ and $\mathbf{g}_{8,0}=8\mathbf{g}_{0,1,0}$, respectively. Using Eq. (6) and the data points from the many-beam formalism, it was found that $A_{\mathbf{g}6,-2}=3.06$ and $A_{\mathbf{g}8,0}=3.22$ keV. For a tilt angle $\theta=8$ mrad, the emission angles are equal to ± 7.44 and ± 3.8 mrad, respectively.

Figure 6(a) shows a CB spectrum for $\theta=8.5$ mrad. The electron transverse momentum is along $\mathbf{g}_{0,1,0}$. The selection is $n=2,4,6,...$ and m is an integer, such that the structure factor $S_{\mathbf{g}n,m}$ of $\mathbf{g}_{n,m}$ is different from zero. This condition leads to a shift of the CB peaks toward the low-energy region (in comparison with the previous scan direction). In this different orientation, no first-order CB corresponds to a momentum transfer along the scan direction. The only momentum transfer (with a nonzero dipole matrix) that results in a photon emission in the forward direction is the vector $4\mathbf{g}_{0,1,0}=\mathbf{g}_{4,0}=\mathbf{g}_p$, which corresponds to a second-order CB [peak labeled $(2')$], while in the previous case this vector corresponded to a first-order CB with, however, a very small dipole matrix. The peak labeled $(1')$ corresponds to two momentum-transfer vectors $\mathbf{g}_{2,\pm 2}$ unlike the previous case where only one vector was transferred to the crystal lattice. Figure 6(b) shows the energy dependence on the tilt angle for the peaks labeled $(1')$, $(2')$, and $(3')$ (third-order CB with

a momentum transfer $\mathbf{g}_{6,\pm 2}$) together with Eq. (6) and the constants $A_{\mathbf{g}n,m}$.

The potential of the ⟨110⟩ axis, which is deeper than that of the ⟨100⟩ axis, is a double-well potential and is due to the axial arrangement in the crystal lattice.[9] Figure 7(a) shows a CB spectrum for $\theta = 8.5$ mrad. The transverse direction was spanned by $\mathbf{g}_{0,0,1} = 2\pi/a_p \mathbf{z}$ and $\mathbf{g}_{1,-1,0} = 2\pi/a_p(\mathbf{x}-\mathbf{y})$. The electron transverse momentum was taken parallel to the vector $\mathbf{g}_p = 4\mathbf{g}_{0,0,1} + 2\mathbf{g}_{1,-1,0}$ [scanned along the $(\bar{1},1,1)$ plane]. The selection that results in a momentum transfer $\mathbf{g}_{n,m} = n\mathbf{g}_{0,0,1} + m\mathbf{g}_{1,-1,0}$ is such that $n+m=2k$, where $k = 1,2,3,4...$ for first, second, third, and fourth order, respectively, and $S_{\mathbf{g}n,m} \neq 0$. The peaks labeled (a), (b), (c), and (d) are the highest peaks for each CB order and correspond to the momenta $\mathbf{g}_{0,2}$, $\mathbf{g}_{4,0}$, $\mathbf{g}_{4,2}$, and $\mathbf{g}_{5,3}$. Only the transfer vector $\mathbf{g}_{4,2}$, which corresponds to a third-order transition, is parallel to the electron transverse momentum. Figure 7(b) shows the photon energy as a function of the tilt angle with the corresponding constants $A_{\mathbf{g}n,m}$. The fourth-order momentum-transfer direction ($\mathbf{g}_{5,3}$) is very close to that of $\mathbf{g}_p$ and therefore the photon emission, for this order, can be approximated with the forward direction.

IV. CONCLUSION

We saw that while planar CB is emitted in the forward direction due to its one-dimensional character, axial CB results in the emission of photons in the forward direction only when the momentum transfer is in the direction of the electron transverse momentum. We saw, in all previous cases, that the energy of the CB peaks varies linearly with the tilt angle. We also saw that in the ⟨100⟩ case, the energy of the CB peaks depends strongly on the direction of the scan, i.e., the electron transverse-momentum direction. The planar and axial CB intensities, for a specific tilt angle, are of the same order. However, the higher CB orders vanish more rapidly in the planar case.

ACKNOWLEDGMENT

A part of this work was carried out under the contract with the Japan Atomic Energy Research Institute.

*Corresponding author. Email address:
khalid@postman.riken.go.jp and
khalid@photon.hepl.hiroshimia-u.ac.jp

[1] J. U. Andersen, Nucl. Instrum. Methods **170**, 1 (1980).
[2] J. U. Andersen, K. R. Eriksen, E. Bonderup, and E. Laegsgaard, Phys. Scr. **24**, 588 (1981).
[3] B. L. Berman *et al.*, Radiat. Eff. Defects Solids **122/123**, 3 (1991).
[4] K. Chouffani, H. Überall, H. Genz, P. Hoffmann Stascheck, U. Nething, and A. Richter, Nucl. Instrum. Methods Phys. Res. B **90**, 133 (1994).
[5] K. Chouffani and H. Überall, Phys. Status Solidi B **213**, 107 (1999).
[6] J. O. Kephart, R. H. Pantell, B. L. Berman, S. Datz, H. Park, and R. K. Klein, Phys. Rev. B **40**, 4249 (1989).
[7] H. Nitta, J. Phys. Soc. Jpn. **59**, 2020 (1990).
[8] K. Chouffani, H. Überall, H. Genz, P. Hoffmann Stascheck, U. Nething, and A. Richter, Nucl. Instrum. Methods Phys. Res. B **152**, 479 (1999).
[9] C. Kittel, *Introduction to Solid State Physics*, 5th ed. (Wiley, New York, 1976)